# Record Energetics for an Inertial Fusion Implosion at NIF

A. B. Zylstra,[1,*] A. L. Kritcher,[1] O. A. Hurricane,[1] D. A. Callahan,[1] K. Baker,[1] T. Braun,[1] D. T. Casey,[1] D. Clark,[1] K. Clark,[2] T. Döppner,[1] L. Divol,[1] D. E. Hinkel,[1] M. Hohenberger,[1] C. Kong,[2] O. L. Landen,[1] A. Nikroo,[1] A. Pak,[1] P. Patel,[1] J. E. Ralph,[1] N. Rice,[2] R. Tommasini,[1] M. Schoff,[2] M. Stadermann,[1] D. Strozzi,[1] C. Weber,[1] C. Young,[1] C. Wild,[3] R. P. J. Town,[1] and M. J. Edwards[1]

[1]*Lawrence Livermore National Laboratory, Livermore, California 94550, USA*
[2]*General Atomics, San Diego, California 92121, USA*
[3]*Diamond Materials Gmbh, 79108 Freiburg, Germany*

(Received 25 August 2020; revised 27 October 2020; accepted 10 December 2020; published 11 January 2021)

Inertial confinement fusion seeks to create burning plasma conditions in a spherical capsule implosion, which requires efficiently absorbing the driver energy in the capsule, transferring that energy into kinetic energy of the imploding DT fuel and then into internal energy of the fuel at stagnation. We report new implosions conducted on the National Ignition Facility (NIF) with several improvements on recent work [Phys. Rev. Lett. **120**, 245003 (2018); Phys. Rev. E **102**, 023210 (2020)]: larger capsules, thicker fuel layers to mitigate fuel-ablator mix, and new symmetry control via cross-beam energy transfer; at modest velocities, these experiments achieve record values for the implosion energetics figures of merit as well as fusion yield for a NIF experiment.

DOI: 10.1103/PhysRevLett.126.025001

Fusion research strives to create plasmas that produce more energy by fusion reactions than is required to create them. This requires satisfying the Lawson criterion [1], which is a power-balance relationship that describes conditions where the fusion power is greater than loss mechanisms and can be written as a temperature-dependent threshold value of the product of plasma pressure ($p$) and energy confinement time ($\tau$). Creating plasmas with fusion energy gain $Q \geq 1$ is the primary goal of flagship facilities, including the magnetic confinement "tokamak" approach at the International Thermonuclear Experimental Reactor [2], in private industry, and in the inertial confinement fusion (ICF) program.

The basic principle of ICF is to use a powerful driver to rapidly compress the fuel to fusion-relevant temperature and density conditions [3]. Most ICF approaches pursue hot-spot ignition [4], in which the fuel is initially layered cryogenically on the inner surface of a capsule. The drive rapidly ablates the capsule material, imparting inwardly directed velocity in the deuterium-tritium (DT) fuel layer, which stagnates at the center creating high pressures in a central "hot spot" created via compression of the initial vapor and ablation of the inner fuel layer. Hot-spot ignition has large theoretical fusion energy gains if the fuel can be compressed symmetrically with low entropy. Multiple driver schemes have been developed including laser indirect drive, where the laser energy is converted to x rays in a radiation cavity ("hohlraum"), laser direct drive [5,6], and magnetic direct drive [7,8]. Significant understanding of these challenges has been developed at the National Ignition Facility (NIF) [9] for the laser indirect drive approach, including successes in implosion control that have led to net gain from the fuel and significant yield amplification from self-heating [10–15]. However, these implosions have reached limitations short of the burning plasma regime [16], and the current program is focused on improving performance toward this milestone.

In this regime where alpha heating approximately balances x-ray losses, the experimental yield ($Y$) follows an analytic scaling [Eq. (25) of Ref. [17]]

$$Y \propto \epsilon^{23/6} \frac{v_{\mathrm{imp}}^{23/3}}{\alpha_{\mathrm{if}}^{12/5}} S^{14/3}, \tag{1}$$

where $\epsilon$ is the efficiency of converting the fuel kinetic energy into internal energy at stagnation, $v_{\mathrm{imp}}$ is the implosion velocity, $\alpha_{\mathrm{if}}$ is the "adiabat," a measure of the in-flight fuel entropy taken as a ratio of the pressure to the Fermi-degenerate pressure, and $S$ is the spatial scale of the implosion. Equation (1) clearly shows that the performance is most sensitive to the implosion velocity, scale, and efficiency, reflecting the underlying fact that the performance is highly dependent on the fuel's kinetic energy and how efficiently that energy is converted to internal energy at stagnation.

In this Letter, we report on implosions using larger-radius capsules to realize the benefit of increased implosion scale ($S$). By fielding these larger capsules at relatively small (~2.7) case to capsule ratio (CCR), we increase the coupling efficiency from laser energy to capsule-absorbed energy while controlling the implosion symmetry using

 

wavelength detuning to control cross-beam energy transfer in the hohlraum. This new design results in record values of the implosion kinetic energy and internal energy of the fuel at stagnation. Our results follow the analytic scaling in Eq. (1) and show a clear route toward further increases in performance.

The capsule is 1100 $\mu$m inner radius, 80 $\mu$m thick, made of nanocrystalline diamond, also known as high-density carbon (HDC). The capsule includes a 23-$\mu$m-thick layer that is doped with 0.3 at.% of W, starting 6.9 $\mu$m from the inner surface, to shield the fuel from preheat and provide a favorable Atwood number at the fuel-ablator interface. On the inside of the capsule, a layer of equimolar DT ice is grown cryogenically with a thickness between 55 and 65 $\mu$m.

The capsule is driven via a radiation bath, generated inside of a high-$Z$ cavity (hohlraum). The cylindrical hohlraum is 11.24 mm in length, 6.4 mm diameter, with 4.0 mm laser entrance holes, made of Au-lined depleted uranium, and filled with 0.3 mg/cm$^3$ of $^4$He gas. The target is driven through the laser entrance holes using four "cones" of beams, in the NIF geometry: the inners at 23.5° and 30° and the outers at 44.5° and 50°, relative to the hohlraum axis. We use a three-shock laser pulse shape with a design adiabat $\alpha \sim 2.5$. The cone fraction, or ratio of the inner power to total power, is designed to be 33%, optimal for NIF, enabling use of NIF's full power and energy (1.9 MJ and 480 TW, respectively).

This design (known as "hybrid E," or HyE) is conceptually similar to previous experiments and is a close iteration the recent hybrid B campaign [18–20], as well as the older "HDC" [12,21,22] and "BigFoot" (BF) [13–15] campaigns; the significant difference from past work is that the CCR is ~2.7, much smaller than previous work (3–3.3 in similar hohlraums). This experiment was designed to have similar implosion characteristics to hybrid B and HDC, specifically the design adiabat and instability growth factors. Maintaining a modest adiabat (~2.5), which results in a high convergence ratio (> 25) relevant to hot-spot ignition, is key to our strategy to increase performance toward a burning plasma [17] with increased capsule-absorbed energy and for realizing possible increases in performance from reduced engineering defects in the future [23].

Decreasing the CCR is advantageous for energy coupling efficiency to the capsule but is much more challenging for low-mode symmetry control, particularly mode 2 [24,25]. We compensate for the intrinsically asymmetric drive, which would result in a highly oblate implosion, by introducing a small amount of wavelength detuning ($\Delta\lambda$) between the inner and outer beams, which transfers energy from the outer to inner cones via cross-beam energy transfer (CBET) [26], increasing drive at the equator. This tactic required large values of $\Delta\lambda$ for high-gas-fill hohlraums [27,28], which exhibited diminishing returns from CBET due to high absorption of inner-beam light before the hohlraum wall and increased Raman scattering on the inner beams. These problems are mitigated in low-gas-fill hohlraums [21,29]; wavelength detuning has been used by plastic-ablator designs in low-fill hohlraums at larger CCR [30,31] and is applied here for the first time to a HDC-ablator design, in a low-gas-filled hohlraum, at an aggressive CCR to improve the implosion energetics. Adjusting the relative laser wavelength by ~1.25 Å in the infrared ($1\omega$) is sufficient to modify CBET, increase the inner-cone power by ~60% according to modeling using VAMPIRE [32], and result in a symmetric implosion for this design (see Ref. [33] and Supplemental Material [34]). Symmetry is inferred from images of x-ray or neutron self-emission from the hot spot; data are shown in Fig. 1. The low-mode symmetry for these shots, inferred from the 17% emission contour (see additional discussion in Supplemental Material [34]), is close to round, with the polar Legendre mode 2, measured by the equatorial detectors [Figs. 1(b) and 1(c)], within ±20% for all shots [35].

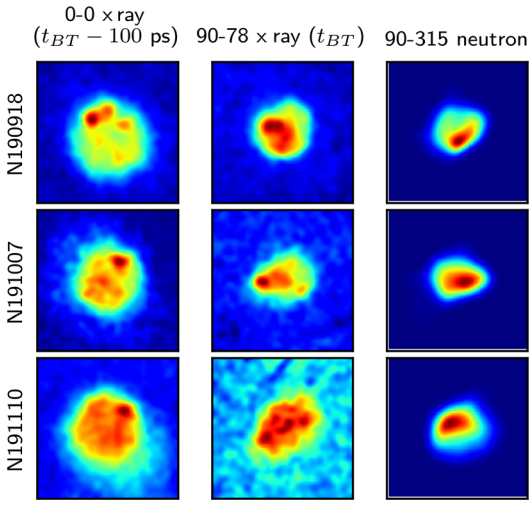


FIG. 1. Implosion self-emission images using x rays (left, center) and neutrons (right). The implosion is viewed from the equator (center, right) or pole (left), and data are taken at either bang time (center, right) or ~100 ps before peak emission (left). Each frame is 200 $\mu$m square, and the viewing angles (e.g., 90-78) are specified as polar and azimuthal angles, respectively.

Table I summarizes these experiments by the shot number (N190918, N191007, and N191110). First, we list the relevant laser parameters including the total energy, peak power, cone fraction, picket energy, and $\Delta\lambda$. The total drive energy is consistent between shots, as well as the cone fraction and picket energy, which are important for low-mode symmetry control [25]. The capsule parameters were very similar between the shots except for the DT cryogenic fuel layer thickness, which was increased on the second and third shots as discussed later. The laser power was increased on the thicker ice shots to compensate for the additional payload mass.

TABLE I. Summary of the hybrid E experiments.

| | | N190918 | N191007 | N191110 |
|---|---|---|---|---|
| Laser | Energy (MJ) | 1.91 | 1.91 | 1.89 |
| | Power (TW) | 467.9 | 491 | 490 |
| | Cone fraction | 0.326 | 0.324 | 0.325 |
| | Picket (kJ) | 60.3 | 56.9 | 57.9 |
| | $\Delta\lambda$ (Å) | 1.25 | 1.25 | 1.35 |
| Capsule | IR ($\mu$m) | 1099.5 | 1099.8 | 1099.6 |
| | Thickness ($\mu$m) | 79.6 | 79.5 | 79.6 |
| | W (%-$\mu$m) | 5.22 | 5.22 | 5.37 |
| | DT layer ($\mu$m) | 56.7 | 65.6 | 65.5 |
| Data | $Y$ ($10^{16}$) | $0.75 \pm 0.03$ | $1.88 \pm 0.06$ | $2.00 \pm 0.05$ |
| | (kJ) | 21 | 53 | 56 |
| | $T_i$ (keV) | $4.43 \pm 0.26$ | $4.52 \pm 0.26$ | $4.54 \pm 0.26$ |
| | DSR (%) | $3.17 \pm 0.13$ | $3.31 \pm 0.16$ | $3.49 \pm 0.15$ |
| | BT (ns) | $9.76 \pm 0.03$ | $9.98 \pm 0.03$ | $10.04 \pm 0.03$ |
| | BW (ps) | $154 \pm 20$ | $151 \pm 20$ | $166 \pm 20$ |
| | Neut. $P_0$ ($\mu$m) | $38.2 \pm 3.8$ | $39.0 \pm 4.2$ | $41.9 \pm 4.3$ |
| | Neut. $P_2/P_0$ | $-0.07 \pm 0.02$ | $-0.21 \pm 0.02$ | $-0.10 \pm 0.01$ |
| Inferred | $v_{\mathrm{imp}}$ (km/s) | $374 \pm 11$ | $374 \pm 11$ | $366 \pm 11$ |
| | Fuel KE (kJ) | $14.5 \pm 0.9$ | $16.7 \pm 1.0$ | $16.0 \pm 1.0$ |
| | HS E (kJ) | $7.0^{+1.3}_{-1.2}$ | $10.9^{+1.9}_{-1.9}$ | $13.1^{+2.3}_{-2.0}$ |
| | P (GBar) | $140^{+27}_{-21}$ | $206^{+31}_{-40}$ | $169^{+25}_{-32}$ |
| Simulated | $Y$ ($10^{16}$) | 3.6 | 2.1 | 1.9 |
| | $T_i$ (keV) | 4.5 | 4.0 | 3.9 |
| | DSR (%) | 3.43 | 3.32 | 3.34 |
| | $v_{\mathrm{imp}}$ (km/s) | 377 | 362 | 358 |
| | Fuel KE (kJ) | 14.5 | 15.4 | 15.0 |
| | HS E (kJ) | 15.7 | 12.3 | 11.5 |
| | P (GBar) | 260 | 210 | 180 |

Key data are summarized in Table I: the total yield in number of neutrons and kilojoules, the ion temperature ($T_i$) [36], measured using neutron time of flight (NTOF) detectors [38,39], the downscattered ratio (DSR), quoted as a $4\pi$ average quantity [40] from measurements using NTOF and the magnetic recoil spectrometer (MRS) [41]. The peak nuclear production time, "bang time" (BT), and burn width (BW) are measured using the gamma reaction history (GRH) [42]. The size ($P_0$) and relative Legendre polar mode 2 symmetry ($P_2/P_0$) are measured using neutron imaging [43].

Next, Table I lists several quantities inferred from the data using simple models [44], including the implosion velocity ($v_{\mathrm{imp}}$), fuel kinetic energy, hot-spot internal energy, and stagnation pressure ($P$). Lastly, Table I shows the same quantities from 1D radiation-hydrodynamics simulations using HYDRA [45] with a fuel preheat model [27] tuned to match the implosion compressibility and drive multipliers tuned to match experimentally measured bang times. The simulated values are consistent with our data-inferred metrics for the energetics, and the clean simulations substantially overpredict the yield for N190918 which was impacted by severe mix, as discussed later. The agreement between this simulation model and the high-performing shots is better than typical for ICF experiments on NIF.

Given the strong scaling of expected performance with velocity [Eq. (1)], it is illustrative to plot the total fusion yield vs velocity, shown in Fig. 2 compared to previous data from campaigns that used HDC ablators [12–15,18–22]. The data are color coded by capsule scale, with curves based on Eq. (1) shown. The older data from the HDC and BF campaigns used smaller-scale capsules and are plotted in shades of blue. High fusion performance was achieved for implosions in those platforms that had high implosion velocities, ~400 km/s, and no other anomalous degradation mechanisms such as higher levels of fuel-ablator mix [46] or low-mode asymmetries. The hybrid B experiments, plotted with scale ~1 in the green-yellow shades, clearly demonstrated the benefit of larger-scale implosions (1000 and 1050 $\mu$m inner radius) at $v_{\mathrm{imp}} \sim 360$ km/s, reaching $\sim 10^{16}$ neutron yields.

This campaign symmetrically imploded even larger capsules than HyB, 1100 $\mu$m. The first experiment, N190918, did not show the expected increase in

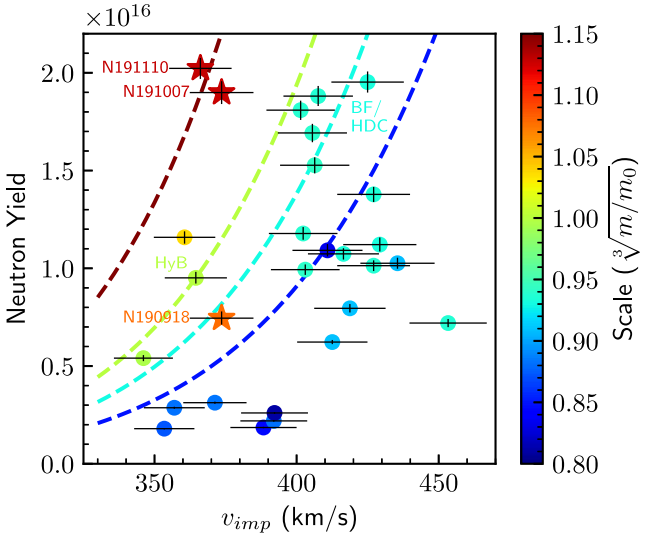


FIG. 2. Fusion yield versus implosion velocity ($v_{\mathrm{imp}}$) for the NIF database of HDC ablator experiments with adequate low-mode symmetry ($P_2/P_0 \leq 0.3$). The data points are color coded by the scale, taken as the cube root of the fuel mass ($m$) relative to N180429 (Ref. [19], $m_0$). Curves of Eq. (1) (also normalized to N180429) at scale $(S) = 0.85$, 0.93, 1.0, and 1.15 are shown. The shots from this campaign are labeled and plotted as stars. The hybrid B campaign are the points in green-yellow, while the largest HDC and BF implosions are cyan.

performance with either scale or velocity: The total yield ($0.75 \times 10^{16}$) was lower than the HyB experiments. N190918 showed clear signatures of high levels of fuel-ablator mix into the hot spot, especially a large number of bright features in x-ray emissivity [46]. These can be seen in Fig. 1, particularly the polar x-ray images taken ~100 ps before bang time. In these images, the fill tube causes a jet that enters the hot spot from the upper right and is visible in all three shots; N190918 shows additional bright emission in the upper left with substantial brightness relative to the fill tube jet. This behavior appeared similar to the HyB campaign experiments that suffered from high levels of mix as reported in Ref. [20] (not shown in Fig. 2).

Ablator material is higher $Z$ than the hydrogenic fusion fuel; mix of ablator material into the fuel is deleterious for fusion performance of ICF implosions on the NIF [20,47–53]. Mix results from hydrodynamic instabilities [23,54–56], largely at the ablation front or fuel-ablator interface. The evolution of a particular initial seed on the capsule is governed by the seed amplitude and the growth factor for modes at the effective wave number of the seed. Since the implosions in the hybrid B and E campaigns have growth factors comparable to the prior subscale experiments that did not suffer from such high levels of mix, we attribute the high levels of mix observed on the N190918 to the much higher levels of initial seeds for instability growth [20], in particular, large numbers of pits on the surface and voids with the bulk material for the capsules used in these shots (see additional details in Supplemental Material [34]).

Instability growth of these initial seeds injects ablator material either into the dense fuel layer, or more damagingly into the hot spot, as indicated by the bright emission features observed. Until higher-quality HDC capsules can be fabricated, high-performing implosions must be designed to be more robust to these defects. To partially mitigate the capsule defects, we tested a thicker DT fuel layer; while this will not intrinsically modify the defects seeds or instability growth, it provides an increased buffer between the mix and the hot spot, which can reduce the most deleterious performance impacts. The second shot in this campaign used a ~10 $\mu$m thicker DT ice layer (see Table I). To compensate for the lower velocity that results from a higher payload mass, we increased the laser peak power. This shot, N191007, used the same capsule batch as N190918 and observed a very large increase in fusion performance, with the yield more than doubling at the same velocity (see Table I and Fig. 2). Previous campaigns with high-quality capsules tested increasing the ice-layer thickness and did not observe a strong increase in yield [14,15]; this result suggests that thicker ice is successfully mitigating the poor capsule quality. On the third shot, N191110, we increased $\Delta\lambda$ to modestly improve the low-mode shape of the implosion (by ~11% in $P_2/P_0$) and used capsules with different seed characteristics. This shot resulted in a new record fusion yield for NIF, of $2 \times 10^{16}$ neutrons or 56 kJ.

The high performance of N191007 and N191110 is a direct result of our platform modifications that significantly improved the energy coupling to the capsule, fuel, and hot spot. Of the ~1.9 MJ of laser energy delivered to the hohlraum, only ~10%–15% is absorbed by the capsule. The majority of the energy absorbed by the capsule is invested in ablation, with only a few percent coupled into the imploded fuel's kinetic energy. Then the incipient hot spot obtains only a fraction of the fuel kinetic energy, with the stagnation less efficient with highly asymmetric or mixed implosions. For example, the data reported in Ref. [12] had ~150 kJ capsule-absorbed energy (~10%). For this design, we couple ~245 kJ, or ~13%, due to the smaller CCR. The coupled energy numbers are calculated from simulation. In terms of capsule-absorbed energy, this is a highly significant increase, comparable to about half the improvement required to reach MJ-class yields according to 3D simulations [23]; cast as a requirement on laser energy for MJ yields, this reduces the 5 MJ requirement of Ref. [23] to ~3 MJ, which is much closer to a proposed upgrade of NIF to 2.6 MJ [57].

Figure 3 shows the inferred fuel kinetic energy and hot-spot energy for a large class of prior NIF experiments. The plot includes data using plastic (CH) ablators [10,11,58,59] and the previously mentioned HDC-ablator campaigns. These shots clearly have the highest values for the fuel kinetic energy, at 15–17 kJ. While N190918 had poor hot-spot energy due to the high levels of mix, N191007 and

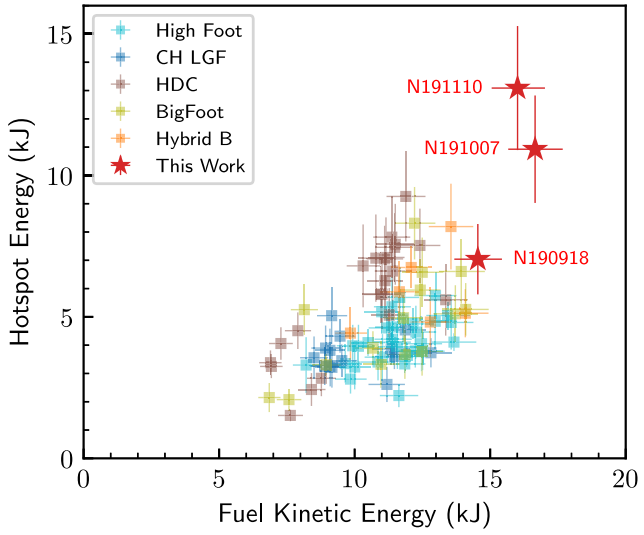


FIG. 3. Energetics for a large number of previous NIF experiments, including plastic (CH) and HDC ablator experiments. The shots in this campaign (HyE) are labeled and plotted as red stars.

N19110 have the highest observed hot-spot energies for NIF and a promisingly high ratio of hot-spot energy to fuel kinetic energy. While these latter two shots have record energetics by a substantial margin, the fusion yield is only slightly higher than the previous record, and the inferred pressures (Table I) are lower than some previous high-performing implosions (e.g., Refs. [12–15,59]). This is because the hybrid E experiments had much lower implosion velocities, which is expected to reduce the pressure and central ion temperature. If these implosions could be accelerated to higher velocities, we would expect a strong increase in performance [15], per Eq. (1) and Fig. 2.

In conclusion, we report on a new design fielded for laser indirect-drive ICF research on the NIF. By reducing the case to capsule ratio, we couple substantially more of the laser energy into the capsule. By controlling asymmetries through judicious use of wavelength detuning to alter the level of cross-beam energy transfer occurring in the hohlraum between the inner and outer beams, the capsule-absorbed energy is efficiently converted to implosion kinetic energy and hot-spot internal energy for a three-shock ignition-relevant design. Mix from defects in the shells introduced during the fabrication process is partially mitigated, for the first time, using a thicker ice layer. The high-performing shots in this campaign achieved record values for the fuel kinetic energy, hot-spot internal energy, and fusion yield on NIF and are in good agreement with our simulation model.

Further increases in performance are possible if additional energy can be coupled to these implosions, especially with a concomitant increase in the implosion velocity. Doing so requires an even more aggressive hohlraum design, which will be studied in future experiments. Mitigating the effect of fuel-ablator mix, which is a major degradation mechanism, is becoming a critical topic for the ICF program as the impact of defects in these larger-scale HDC capsules becomes apparent [20]. Our data show that thicker ice layers are an effective buffer against this mix, a significant result both toward implosion designs that are naturally more robust to instability growth and to benchmark new highly resolved mix modeling in 3D implosion simulations [23], until the manufacturing process can be improved to reduce or eliminate these defects. These data suggest a route toward further increases in performance toward the burning plasma regime on NIF.

We thank the operations, engineering, and target fabrication staff at the NIF for supporting these experiments. This work was performed under the auspices of the U.S. Department of Energy by Lawrence Livermore National Laboratory under Contract No. DE-AC52-07NA27344, and by General Atomics under Contract No. 89233119CNA000063. This document was prepared as an account of work sponsored by an agency of the U.S. government. Neither the U.S. government nor Lawrence Livermore National Security, LLC, nor any of their employees makes any warranty, expressed or implied, or assumes any legal liability or responsibility for the accuracy, completeness, or usefulness of any information, apparatus, product, or process disclosed, or represents that its use would not infringe privately owned rights. The views and opinions of authors expressed herein do not necessarily state or reflect those of the U.S. government or Lawrence Livermore National Security, LLC, and shall not be used for advertising or product endorsement purposes.

*zylstra1@llnl.gov

[1] J. D. Lawson, Proc. Phys. Soc. London Sect. B **70**, 6 (1957).
[2] B. J. Green, and ITER International Team and Partici Teams, Plasma Phys. Controlled Fusion **45**, 687 (2003).
[3] J. Nuckolls, L. Wood, A. Thiessen, and G. Zimmerman, Nature (London) **239**, 139 (1972).
[4] J. Lindl, Phys. Plasmas **2**, 3933 (1995).
[5] R. L. McCrory *et al.*, Phys. Plasmas **15**, 055503 (2008).
[6] R. S. Craxton *et al.*, Phys. Plasmas **22**, 110501 (2015).
[7] S. A. Slutz, M. C. Herrmann, R. A. Vesey, A. B. Sefkow, D. B. Sinars, D. C. Rovang, K. J. Peterson, and M. E. Cuneo, Phys. Plasmas **17**, 056303 (2010).
[8] M. R. Gomez, S. A. Slutz, A. B. Sefkow, D. B. Sinars, K. D. Hahn *et al.*, Phys. Rev. Lett. **113**, 155003 (2014).
[9] G. Miller, E. Moses, and C. Wuest, Nucl. Fusion **44**, S228 (2004).
[10] O. Hurricane *et al.*, Nature (London) **506**, 343 (2014).
[11] O. A. Hurricane *et al.*, Nat. Phys. **12**, 800 (2016).
[12] S. Le Pape, L. F. Berzak Hopkins, L. Divol, A. Pak, E. L. Dewald *et al.*, Phys. Rev. Lett. **120**, 245003 (2018).
[13] D. T. Casey *et al.*, Phys. Plasmas **25**, 056308 (2018).
[14] K. L. Baker, C. A. Thomas, D. T. Casey, S. Khan, B. K. Spears *et al.*, Phys. Rev. Lett. **121**, 135001 (2018).

[15] K. L. Baker, C. A. Thomas, D. T. Casey, M. Hohenberger, S. Khan *et al.*, Phys. Rev. E **102**, 023210 (2020).
[16] O. A. Hurricane *et al.*, Phys. Plasmas **26**, 052704 (2019).
[17] O. Hurricane *et al.*, Plasma Phys. Controlled Fusion **61**, 014033 (2019).
[18] A. L. Kritcher *et al.*, Phys. Plasmas **27**, 052710 (2020).
[19] M. Hohenberger *et al.*, Phys. Plasmas **27**, 112704 (2020).
[20] A. B. Zylstra *et al.*, Phys. Plasmas **27**, 092709 (2020).
[21] L. Divol *et al.*, Phys. Plasmas **24**, 056309 (2017).
[22] L. B. Hopkins *et al.*, Phys. Plasmas **25**, 080706 (2018).
[23] D. S. Clark *et al.*, Phys. Plasmas **26**, 050601 (2019).
[24] J. E. Ralph *et al.*, Phys. Plasmas **25**, 082701 (2018).
[25] D. A. Callahan *et al.*, Phys. Plasmas **25**, 056305 (2018).
[26] P. Michel *et al.*, Phys. Plasmas **17**, 056305 (2010).
[27] A. L. Kritcher *et al.*, Phys. Plasmas **23**, 052709 (2016).
[28] D. S. Clark *et al.*, Phys. Plasmas **23**, 056302 (2016).
[29] L. F. Berzak Hopkins *et al.*, Phys. Rev. Lett. **114**, 175001 (2015).
[30] A. L. Kritcher *et al.*, Phys. Rev. E **98**, 053206 (2018).
[31] L. A. Pickworth *et al.*, Phys. Plasmas **27**, 102702 (2020).
[32] A. Colaïtis, T. Chapman, D. Strozzi, L. Divol, and P. Michel, Phys. Plasmas **25**, 033114 (2018).
[33] R. Tommasini *et al.* (to be published).
[34] See Supplemental Material at http://link.aps.org/supplemental/10.1103/PhysRevLett.126.025001 for a detailed description of polar symmetry measurements and control via cross-beam energy transfer, as well as details on defects present for capsules used in this work.
[35] A. L. Kritcher *et al.*, Phys. Plasmas **21**, 042708 (2014).
[36] The ion temperatures reported in this work are the minimum measured temperature inferred from the width of the DT neutron spectrum across several lines of sight. The spectral width can be inflated by residual kinetic energy [37], the impact of which is reduced by reporting the minimum value.
[37] T. Murphy, Phys. Plasmas **21**, 072701 (2014).
[38] V. Y. Glebov *et al.*, Rev. Sci. Instrum. **81**, 10D325 (2010).
[39] R. Hatarik *et al.*, J. Appl. Phys. **118**, 184502 (2015).
[40] D. T. Casey (private communication).
[41] D. Casey *et al.*, Rev. Sci. Instrum. **84**, 043506 (2013).
[42] H. W. Herrmann *et al.*, Rev. Sci. Instrum. **81**, 10D333 (2010).
[43] P. Volegov *et al.*, Rev. Sci. Instrum. **85**, 023508 (2014).
[44] P. K. Patel *et al.*, Phys. Plasmas **27**, 050901 (2020).
[45] M. M. Marinak, G. D. Kerbel, N. A. Gentile, O. Jones, D. Munro, S. Pollaine, T. R. Dittrich, and S. W. Haan, Phys. Plasmas **8**, 2275 (2001).
[46] A. Pak, L. Divol, C. R. Weber, L. F. B. Hopkins, D. S. Clark *et al.*, Phys. Rev. Lett. **124**, 145001 (2020).
[47] B. A. Hammel *et al.*, Phys. Plasmas **18**, 056310 (2011).
[48] S. P. Regan *et al.*, Phys. Plasmas **19**, 056307 (2012).
[49] S. P. Regan, R. Epstein, B. A. Hammel, L. J. Suter, H. A. Scott *et al.*, Phys. Rev. Lett. **111**, 045001 (2013).
[50] M. J. Edwards *et al.*, Phys. Plasmas **20**, 070501 (2013).
[51] T. Ma *et al.*, Phys. Rev. Lett. **111**, 085004 (2013).
[52] T. Ma *et al.*, Phys. Plasmas **24**, 056311 (2017).
[53] A. B. Zylstra *et al.*, Phys. Plasmas **26**, 052707 (2019).
[54] D. S. Clark, S. W. Haan, A. W. Cook, M. J. Edwards, B. A. Hammel, J. M. Koning, and M. M. Marinak, Phys. Plasmas **18**, 082701 (2011).
[55] C. R. Weber *et al.*, Phys. Rev. Lett. **117**, 075002 (2016).
[56] D. Clark, A. Kritcher, S. Yi, A. Zylstra, S. Haan, and C. Weber, Phys. Plasmas **25**, 032703 (2018).
[57] J. M. Di Nicola *et al.*, Nucl. Fusion **59**, 032004 (2019).
[58] D. E. Hinkel, L. F. Berzak Hopkins, T. Ma, J. E. Ralph, F. Albert *et al.*, Phys. Rev. Lett. **117**, 225002 (2016).
[59] T. Döppner *et al.*, Phys. Plasmas **27**, 042701 (2020).